
SynapsNet: Enhancing Neuronal Population Dynamics Modeling via Learning Functional Connectivity

Parsa Delavari
Neuroscience
University of British Columbia
parsadlr@student.ubc.ca

Ipek Oruc
Ophthalmology and Visual Sciences
University of British Columbia
ipor@mail.ubc.ca

Timothy H Murphy
Psychiatry
University of British Columbia
thmurphy@mail.ubc.ca

Abstract

The availability of large-scale neuronal population datasets necessitates new methods to model population dynamics and extract interpretable, scientifically translatable insights. Existing deep learning methods often overlook the biological mechanisms underlying population activity and thus exhibit suboptimal performance with neuronal data and provide little to no interpretable information about neurons and their interactions. In response, we introduce SYNAPSNET, a novel deep-learning framework that effectively models population dynamics and functional interactions between neurons. Within this biologically realistic framework, each neuron, characterized by a latent embedding, sends and receives currents through directed connections. A shared decoder uses the input current, previous neuronal activity, neuron embedding, and behavioral data to predict the population activity in the next time step. Unlike common sequential models that treat population activity as a multichannel time series, SYNAPSNET applies its decoder to each neuron (channel) individually, with the learnable functional connectivity serving as the sole pathway for information flow between neurons. Our experiments, conducted on mouse cortical activity from publicly available datasets and recorded using the two most common population recording modalities—Ca imaging and Neuropixels—across three distinct tasks, demonstrate that SYNAPSNET consistently outperforms existing models in forecasting population activity. Additionally, our experiments on both real and synthetic data showed that SYNAPSNET accurately learns functional connectivity that reveals predictive interactions between neurons.

1 Introduction

Recent advancements in brain recording techniques have enabled simultaneous in-vivo recordings from hundreds of neurons. This availability of neuronal population activity has motivated numerous studies on population dynamics, which can address neuroscientific questions such as explaining brain function and behavior (Vyas et al., 2020; Gallego et al., 2020), as well as brain decoding applications like brain-computer interfaces (BCIs) (Willett et al., 2023; Heelan et al., 2019). Various approaches for studying neural dynamics have been proposed in the literature, including neural manifolds (Duncker & Sahani, 2021) and latent variable models (LVMs) (Pandarinath et al., 2018; Nolan et al., 2022), which aim to capture low-dimensional patterns in neural activity by reproducing this activity. However, recent evidence suggests that neural activity forecasting offers great potential for

studying population dynamics and capturing causal interactions in neural activity, making forecasting a promising approach for studying neural dynamics (Li et al., 2024).

Although analyzing neuronal population dynamics holds immense potential for neuroscientific research and applications, the data is typically large, acquired from multiple animals across numerous recording sessions, necessitating novel and scalable methods for analysis and interpretation (Paninski & Cunningham, 2018; Hurwitz et al., 2021). Deep learning models have been extensively applied to neural data to address this need (Richards et al., 2019; Paninski & Cunningham, 2018). However, these methods often face significant limitations, particularly in neuroscience applications. Firstly, they typically offer minimal interpretability, providing little insight into the brain’s underlying mechanisms. Ideally, explainable deep learning models could harness computational power to decode vast amounts of data, with their interpretability guiding scientists toward scientific discovery, as demonstrated in successful cases (Lemos et al., 2023; Delavari et al., 2023). Secondly, many deep learning approaches neglect the underlying biological mechanisms (Kietzmann et al., 2017), limiting their performance by applying generic architectures adapted from other domains to neural data. These limitations highlight the need for more biologically informed and interpretable models of neuronal population dynamics.

One potential biological prior that can be incorporated in the models’ architecture is functional connectivity (FC). Functional connectivity refers to the statistical dependencies between distinct neurons/regions in the brain, indicating how they communicate and coordinate with each other during various cognitive tasks and resting states (Friston, 2011). FC analysis has been utilized in a wide range of studies, including those on brain diseases and disorders (Du et al., 2018; Sheline & Raichle, 2013), brain representation learning (Behrouz et al., 2024), brain classification (Riaz et al., 2020; Du et al., 2018), and in particular neural data forecasting (Li et al., 2024). There are various methods to infer functional connectivity across different recording modalities (Marzetti et al., 2019; Yu, 2020; Li et al., 2009) including spiking data (Perich et al., 2020; Ulló et al., 2014; Pastore et al., 2018; Quinn et al., 2011), however, each of the existing methods for inferring FC has a subset of the following limitations. They often measure only simple statistical similarities between source and target units, overlook causal interactions that are not necessarily symmetric, lack generalizability to unseen population activity, and are not flexible enough to account for multi-synaptic interactions occurring over varying delays. These challenges underscore the need for advanced methods that can more accurately capture the complex interactions within neural populations.

In this work, we introduce SYNAPSNET, a biologically inspired deep learning framework designed to model neuronal populations while uncovering functional connectivity. It integrates past neural activity, input currents from connected neurons, intrinsic neuron properties, and behavioral states to predict neural dynamics. This model builds upon previous work (Mi et al., 2024) to implicitly model dynamics of individual neurons and learns functional connectivity to capture directed interactions between neurons. We validate SYNAPSNET through extensive experiments on both synthetic and real datasets of mouse cortical activity recorded via the most common population recording methods, calcium imaging and Neuropixels (Jun et al., 2017). Our experiments demonstrate that SYNAPSNET outperforms conventional time-series models in predicting neural activity showcasing its high capability of capturing population dynamics. Also, SYNAPSNET provides insights into the underlying interactions between neurons by accurately inferring functional connectivity.

2 SYNAPSNET

2.1 Overview

The aim of SYNAPSNET is to develop an interpretable model of neuronal populations capable of predicting future dynamics based on the current and past states of the brain and behavior. To this end, our model employs a biologically inspired framework in which a dynamical model predicts the future activity of each neuron by taking: ① its past activity, ② the input currents coming from the connected neurons, ③ the intrinsic properties of the target neuron, and ④ the animal’s behavioral state (e.g., running speed). We use these components as previous research confirm their role on neuronal responses. The Hodgkin-Huxley equations (Hodgkin & Huxley, 1952), a foundational work in computational neuroscience, describe a neuron’s membrane potential dynamics as a function of its current voltage, input currents from presynaptic neurons, and a set of neuron-specific physiological properties. Additionally, behavior has been shown to significantly impact neural responses, with the first principal components of single-trial population activity corresponding to behavioral variables

such as running speed and pupil size in various brain regions, including the visual cortex (Stringer et al., 2019).

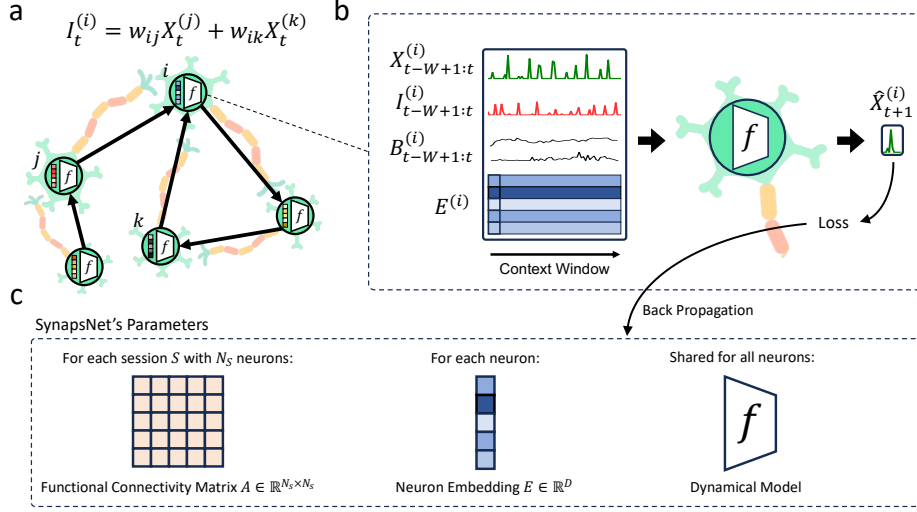


Figure 1: SYNAPSNET overview. (a) The functional connectivity defined between neurons on the model and how input current is inferred based on functional connectivity and population activity (b) An example input frame to the dynamical model which includes past activity over the context window, past input current, past behavioral data, and the unique embedding of the target neuron. (c) The three sets of parameters in SYNAPSNET: adjacency matrix A for each session, embedding vector E for each neuron, and dynamical model.

Although the Hodgkin-Huxley point-neuron model can accurately predict neuron dynamics, it requires detailed information on the activity of all presynaptic neurons, their synaptic strengths, and an exhaustive physiological description of the neurons. This level of detail is nearly impossible to obtain with current population recording techniques, which typically capture only a limited subset of neurons and provide minimal to no information on the population’s physiological and anatomical properties. In this context, functional connectivity has been used as an alternative to anatomical connectivity for modeling interactions between neurons (Poli et al., 2015). These functional interactions, which can be inferred from population activity, have been shown to predict neural responses even when only a small number of neurons are recorded (Stevenson et al., 2012). Therefore, we estimate each neuron’s input current based on the activity of other neurons and the population’s functional connectivity. To address the lack of detailed physiological features of neurons, we use NeuPRINT (Mi et al., 2024) to learn time-invariant embeddings for each neuron based solely on population activity. The innovative approach proposed in NeuPRINT removes the dependency on neuron-specific characteristics from the dynamical model, placing it in the input so that the dynamical model becomes independent of intrinsic properties and can be shared across all neurons.

2.2 Implementation

We represent population datasets as a set of recording sessions \mathbb{S} , where each session $S_j \in \mathbb{S}$ includes a set of recorded neurons \mathcal{N}_j , population activity over time $X_j \in \mathbb{R}^{|\mathcal{N}_j| \times T}$, and available behavioral data over time $B_j \in \mathbb{R}^{N_B \times T}$. Let $M = |\bigcup_{j=1}^{|\mathbb{S}|} \mathcal{N}_j|$ be the total number of unique neurons across all recording sessions, acknowledging that some neurons may appear in multiple sessions. We define three sets of learnable parameters in SYNAPSNET (Figure 1c): ① neuron embeddings $E \in \mathbb{R}^{M \times D}$, where D is the dimensionality of the embedding vectors, ② functional connectivity matrices $\{A_j\}_{j=1}^{|\mathbb{S}|}$, where $A_j \in \mathbb{R}^{|\mathcal{N}_j| \times |\mathcal{N}_j|}$, and ③ a dynamical model $f(\cdot)$ shared among all neurons across all sessions. For simplicity, we drop the session number subscript j in the following descriptions and provide expressions for a single session.

Inferred input current calculation. Using population activity and functional connectivity, we calculate the input current to neuron i at time t as $I_t^{(i)} = \sum_{k=1}^{|\mathcal{N}|} A^{(i,k)} X_t^{(k)}$ (Figure 1a).

Dynamical model. We express the neuronal dynamics as

$$\hat{X}_{t+1}^{(i)} = f(X_{t-W+1:t}^{(i)}, I_{t-W+1:t}^{(i)}, B_{t-W+1:t}, E^{(i)})$$

where W is the context window that determines the history considered by the dynamical model (Figure 1b). The dynamical model f can be any sequential model designed for processing time-series data. The results presented in this paper are obtained using a GRU (Cho et al., 2014) (for results with other sequential models, see the supplementary materials).

Training. We formulate an optimization problem using the loss \mathcal{L} , calculated based on the ground truth and predicted activity, to learn the three sets of parameters in SYNAPSNET:

$$\min_{f, \{A_j\}_j, E} \left(\mathbb{E}_X \left[\mathcal{L}(\hat{X}_{t+1}^{(i)}, X_{t+1}^{(i)}) \right] + \lambda \sum_j \|A_j\|_2 \right)$$

where $\mathcal{L}(\cdot)$ is mean squared error (MSE), λ is the regularization weight for preventing overfitting through $\{A_j\}_j$ and $\|\cdot\|_2$ denotes L2 norm. For more details about the training procedure and the hyperparameters used, please refer to the supplementary materials.

3 Experiments

3.1 Population Activity Forecasting

We evaluate SYNAPSNET’s performance in forecasting neuronal population activity using two distinct public datasets: Bugeon et al. (2022) and Siegle et al. (2021).

Datasets and Preprocessing

The dataset from Bugeon et al. (2022) consists of two-photon calcium imaging data recorded from the mouse primary visual cortex (V1). Mice were exposed to three types of visual stimuli: natural scenes, drifting gratings, and blank screens (spontaneous activity). This dataset includes calcium traces from four mice, recorded across 17 sessions of approximately 20 minutes each. Each session captured between 178 and 868 neurons, totaling 9728 neurons. Neurons were recorded at a 4.3 Hz sampling rate on 7 imaging planes at different cortical depths, resulting in volumetric recordings. The dataset also provides neuron positions, cell types, and behavioral data such as running speed and pupil size. We normalized each neuron’s calcium trace and behavioral variables.

The dataset from Siegle et al. (2021) includes electrophysiology spiking data from mouse cortical neurons, recorded using six Neuropixels probes (Jun et al., 2017). This dataset primarily covers V1 and higher visual areas, as well as deep subcortical areas like the LGN and hippocampus CA1. It features two session types: "brain observatory" sessions for natural scenes and drifting gratings, and "functional connectivity" sessions for spontaneous activity (blank screen). We included sessions where neuron locations were available, resulting in 46 sessions (46 animals) and 31,408 recorded neurons. The dataset also provides running speed data. We binned the spikes with a 33.3 ms bin width and normalized each neuron’s response and behavioral data.

Benchmark Models

We compare SYNAPSNET with the following existing models: standard sequential models (RNN Elman (1990), GRU Cho et al. (2014), LSTM Hochreiter & Schmidhuber (1997)); NeuPRINT Mi et al. (2024), a self-supervised method of learning neuronal representations based on population dynamics; LFADSPandarath et al. (2018), an RNN based variational auto-encoder designed specifically for neuronal population dynamics; GWNet Wu et al. (2019), a graph neural network designed to model both spatial interactions and temporal patterns in data. Each sequential model was trained separately on every session due to varying model and input sizes based on recorded neurons. NeuPRINT

and SYNAPSNET were trained on multiple sessions and animals due to their design, allowing the dynamical model to operate at the single-neuron level. For a fair comparison, we trained NeuPRINT and SYNAPSNET on both single-session data and the entire dataset, reporting results separately.

Evaluation on Population Activity Forecasting

We assessed SYNAPSNET and the benchmark models on two different data modalities across three tasks. We measured test MSE loss and Pearson’s correlation between true and predicted population activity, averaging over all times for each neuron and across all neurons in each recording session. The means and standard errors were calculated across sessions (Ca imaging: $n = 17$; Neuropixels natural scenes and drifting gratings: $n = 22$; Neuropixels spontaneous: $n = 24$). Performance measures are summarized in Table 1.

NeuPRINT outperformed the conventional time-series models, highlighting the advantage of modeling dynamics at the single-neuron level over treating the population activity as multichannel time-series data. This may be due to the sparse and stochastic nature of spiking activity, which complicates population-level analysis. SYNAPSNET consistently surpassed other general models, including NeuPRINT, across both data modalities and all three tasks, demonstrating its superior capability in modeling neuronal population dynamics. Both NeuPRINT and SYNAPSNET demonstrated improved performance when trained on multiple sessions, indicating their scalability. SYNAPSNET achieved approximately 15% higher correlation scores compared to the general models and 5% higher compared to NeuPRINT on calcium imaging data, translating to around 80% and 15% relative improvements, respectively. For the Neuropixels modality, these values were about 8% and 3%, corresponding to approximately 30% and 15% relative improvements. Notably, SYNAPSNET exhibited greater improvements on tasks involving visual stimuli compared to spontaneous activity, highlighting the importance of stimulus-driven functional connectivity inferred by the model.

Table 1: Performance on neural data forecasting. Mean correlation and loss (%) \pm standard error of the mean[†].

Data Modality	Model	Natural Scenes		Drifting Gratings		Spontaneous	
		Corr(%) \uparrow	Loss \downarrow	Corr(%) \uparrow	Loss \downarrow	Corr(%) \uparrow	Loss \downarrow
Ca Imaging	RNN	24.09 \pm 0.88	0.920 \pm 0.040	19.95 \pm 0.81	1.017 \pm 0.050	13.15 \pm 0.75	0.924 \pm 0.017
	GRU	24.21 \pm 0.87	0.915 \pm 0.040	20.08 \pm 0.89	1.009 \pm 0.049	13.31 \pm 0.85	0.920 \pm 0.017
	LSTM	24.60 \pm 0.87	0.911 \pm 0.040	20.47 \pm 0.85	1.006 \pm 0.049	13.97 \pm 0.90	0.917 \pm 0.017
	LFADS	25.70 \pm 0.73	1.056 \pm 0.040	22.96 \pm 0.62	1.138 \pm 0.049	12.33 \pm 0.79	0.941 \pm 0.017
	GWNET	33.04 \pm 0.87	0.829 \pm 0.040	29.89 \pm 0.85	0.910 \pm 0.049	28.20 \pm 0.90	0.874 \pm 0.017
	NEUPRINT	33.82\pm0.85	0.884\pm0.039	31.17\pm1.00	0.973\pm0.052	28.82\pm1.25	0.867\pm0.015
	SYNAPSNET	37.43\pm1.05	0.846\pm0.037	36.14\pm1.05	0.927\pm0.48	30.60\pm1.29	0.855\pm0.016
	NEUPRINT (multi-session)	34.16 \pm 0.91	0.865 \pm 0.038	31.64 \pm 1.38	1.045 \pm 0.014	29.25 \pm 1.43	0.903 \pm 0.014
	SYNAPSNET (multi-session)	37.94\pm1.15	0.825\pm0.035	36.79\pm1.62	0.992\pm0.015	31.60\pm1.58	0.886\pm0.015
	NeuroPixels	RNN	18.50 \pm 0.30	0.963 \pm 0.012	20.20 \pm 0.35	0.992 \pm 0.032	16.67 \pm 0.44
GRU		18.11 \pm 0.32	0.963 \pm 0.012	20.33 \pm 0.37	0.989 \pm 0.032	16.68 \pm 0.47	0.989 \pm 0.015
LSTM		18.02 \pm 0.33	0.963 \pm 0.012	20.39 \pm 0.39	0.987 \pm 0.031	16.74 \pm 0.47	0.987 \pm 0.015
LFADS		18.26 \pm 0.73	0.987 \pm 0.040	20.65 \pm 0.62	0.953 \pm 0.049	17.38 \pm 0.79	0.927 \pm 0.017
GWNET		21.10 \pm 0.87	0.949 \pm 0.040	22.54 \pm 0.85	0.935 \pm 0.049	20.21 \pm 0.90	0.941 \pm 0.017
NEUPRINT		21.68\pm0.21	0.942\pm0.011	22.93\pm0.25	0.967\pm0.029	20.79\pm0.48	0.967\pm0.014
SYNAPSNET		24.38\pm0.28	0.926\pm0.011	25.55\pm0.31	0.953\pm0.029	22.51\pm0.53	0.953\pm0.014
NEUPRINT (multi-session)		22.10 \pm 0.19	0.951 \pm 0.012	23.49 \pm 0.31	0.941 \pm 0.011	21.31 \pm 0.42	0.919 \pm 0.014
SYNAPSNET (multi-session)		25.48\pm0.23	0.932\pm0.012	26.80\pm0.081	0.921\pm0.011	23.83\pm0.44	0.905\pm0.014

[†] The bold values correspond to the best performance metric separately for multi-/single-session training and each data modality. Blue cells indicate significant difference with the next best-performing model (p -value ≤ 0.05 achieved by paired- t -tests).

We also assessed the performance of SYNAPSNET at the population level. Figure 2 compares the first three principal components (PCs) of the true and predicted population activity. Across all sessions, SYNAPSNET’s predictions achieved mean correlation scores of approximately 85%, 75%, and 65% for the first three PCs, respectively. These correlations were significantly higher than those achieved by NeuPRINT.

Ablation Study

We conducted ablation experiments on SYNAPSNET by removing each of its main components. The results, presented in Table 2, indicate that removing functional connectivity leads to the most significant increase in test loss across both data modalities. Furthermore, the model without functional connectivity exhibits the lowest correlation score on the Neuropixels dataset and nearly matches the

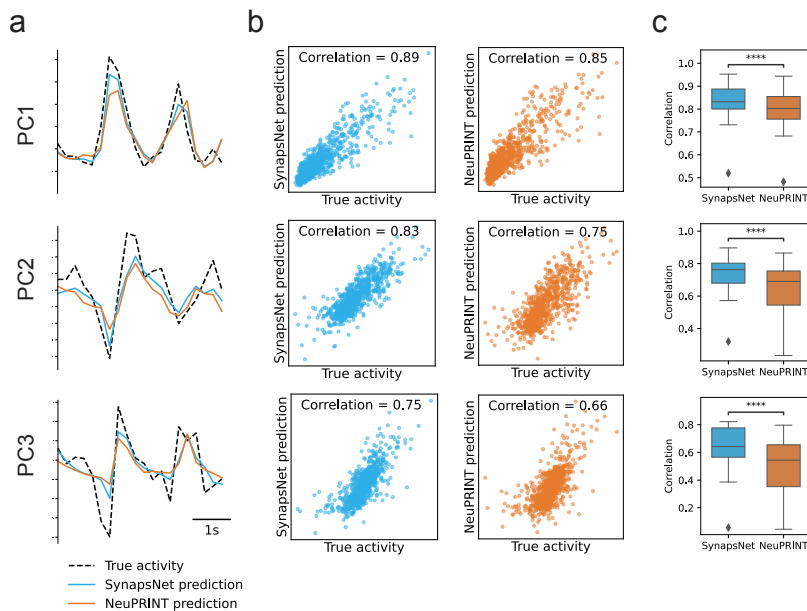


Figure 2: Performance on neural data forecasting. (a) The first three principal components (PCs) of the true and predicted population activity sampled from an example session. (b) Correlation between the first three PCs of the true and predicted activity for the all-time points in the test set of an example session. (c) Comparison between prediction correlations achieved by SynapsNet and NeuPRINT across the test portion of all sessions. **** indicates p -value $\leq .0001$ achieved by paired- t -test.

lowest correlation score on the calcium imaging data. These results suggest the significant role of functional connectivity in capturing the population dynamics.

Table 2: Ablation experiments on neural data forecasting. Mean correlation and loss (%) \pm standard error of the mean[†].

Data Modality	Model	Natural Scenes	
		<i>Corr</i> (%) \uparrow	<i>Loss</i> \downarrow
Ca Imaging	SYNAPSNET	37.94 \pm 1.15	0.825 \pm 0.035
	Without Neuronal Embeddings	35.96 \pm 1.04	0.836 \pm 0.035
	Without Previous Activity	33.27\pm1.22	0.851 \pm 0.036
	Without Functional Connectivity	33.94.09 \pm 0.867	0.920\pm0.038
NeuroPixels	SYNAPSNET	25.48 \pm 0.23	0.932 \pm 0.012
	Without Neuronal Embeddings	24.68 \pm 0.23	0.933 \pm 0.009
	Without Previous Activity	24.59 \pm 0.24	0.933 \pm 0.010
	Without Functional Connectivity	21.85\pm0.22	0.949\pm0.009

[†] The bold values correspond to the largest drop in the performance metric separately for multi-/single-session training and each data modality.

Evaluating Functional Connectivity Learned by SYNAPSNET

Figure 3a presents the functional connectivity (FC) matrices inferred by SYNAPSNET alongside the pair-wise correlations between neurons in two example sessions—one from calcium imaging and the other from the Neuropixels dataset. SYNAPSNET’s inferred FC matrices appear sparser, more asymmetric, and more structured compared to the correlation matrices. Figure 3b offers a 3D visualization of neurons and the learned connections, revealing clear patterns of connection types and

strengths based on neuron locations, even though neuron positions were not provided to the model during training.

Additionally, we analyzed the input currents inferred by SYNAPSNET, which are latent variables used to predict future neural activity. As described in §2.2, we calculated input currents based on population activity and functional connectivity within a recording session using the equation $I = AX$ (Figure 4a). We then measured the cross-correlation (correlation as a function of relative delay) between the input current to each neuron and its activity. We employed three different methods to infer functional connectivity: SYNAPSNET, pair-wise correlation, and shuffled SYNAPSNET’s FC. As illustrated in Figure 4b, the cross-correlation curve peaks at a positive delay, indicating that the input current is most correlated with future activity, demonstrating a predictive relationship. In contrast, the FC derived from pair-wise correlation peaks at a delay of zero. Notably, in the forecasting task, predicting activity at time t relies solely on information up to time $t - 1$, making current and future time points inaccessible. Interestingly, the input currents derived by SYNAPSNET show a higher correlation with population activity at positive delays compared to the pair-wise correlation method, which are the only time points available in forecasting.

Despite these promising results, evaluating learned functional connectivity remains challenging without access to ground-truth neuron connectivity. Therefore, we conducted an experiment using synthetic data simulated with known functional connectivity to further assess SYNAPSNET’s ability to capture functional dependencies in the data.

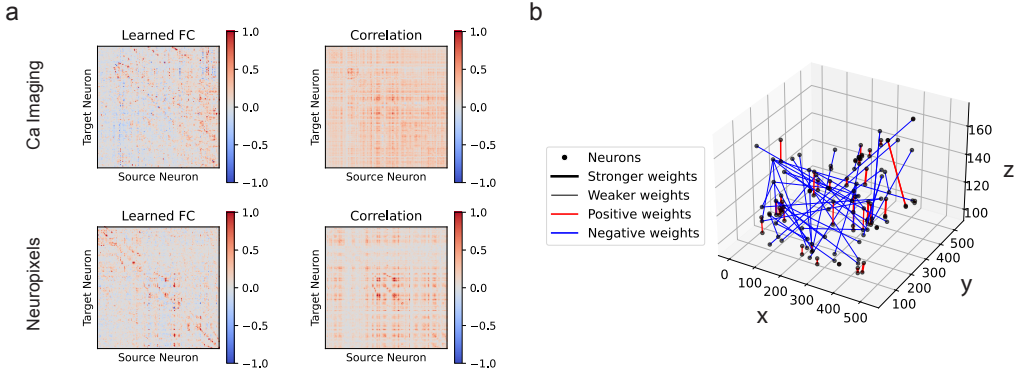


Figure 3: Illustration of the learned functional connectivity. (a) The connectivity matrix learned by SYNAPSNET compared with that of achieved by pair-wise Pearson’s correlation. The top and bottom matrices correspond to a sample session from Ca imaging and Neuropixels modalities respectively. (b) 3D visualization of the learned functional connectivity by SYNAPSNET on a sample Ca imaging session. Dots represent neurons and lines show the type and strength of the connections. Coordinates are in μm .

3.2 Evaluation of Learned Functional Connectivity on Synthetic Data

Simulation

To further validate SYNAPSNET’s ability to recover functional interactions, we simulated the activity of a neuron population with known ground-truth connectivity (Figure 5a). We simulated 600 interconnected neurons with connection weights randomly initialized to create a sparse connectivity matrix A^1 . We generated four random variables, two representing behavioral data (B) and two representing task variables (V). Each neuron’s firing rate was calculated as: $R_t^{(i)} = \sigma \left(\bar{R}^{(i)} + w_1 \sum_k A^{(i,k)} X_{t-1}^{(k)} + w_2 B_{t-1} + w_3 V_{t-1} - w_4 X_{t-1}^{(i)} + n_t \right)$ where $\sigma(\cdot)$ is the nonlinearity (\tanh here), \bar{R} is the neuron’s mean firing rate, n_t is noise. Parameters w_1 to w_4 control the effect of input current, behavior, task, and self-inhibition respectively, and are randomly initialized for each

¹For better visual comparison, the locations of non-zero elements in the connectivity matrix were based on an image from the Mandelbrot set fractal to include visual patterns in the ground-truth adjacency matrix.

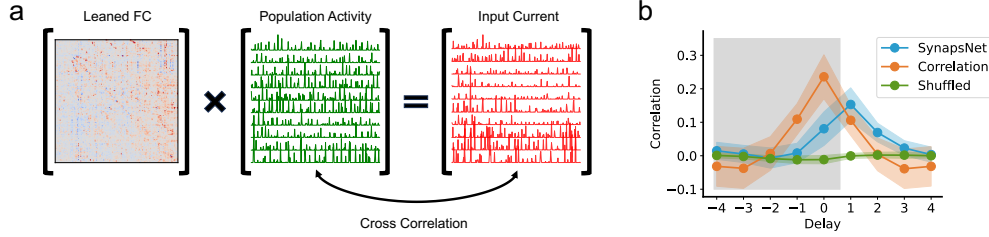


Figure 4: Input currents achieved by functional connectivity. (a) An example calculation of the input current to each neuron based on the population activity and the learned functional connectivity. (b) Average cross-correlations between each neuron’s input currents and their activity. The input currents are calculated based on connectivity matrices achieved by three different methods: SYNAPSNET, pair-wise correlation, and shuffling the SYNAPSNET’s connectivity matrix. The dots and color-shaded areas represent the mean and standard deviation of the correlations. The x-axis shows delays in time steps and the gray-shaded area marks the unavailable time points during the neuron activity forecasting task.

neuron. Then, the activity of each neuron is determined by a Poisson process: $X_t^{(i)} \sim \text{Poisson}(R_t^{(i)})$. Finally, a subset of 200 neurons is randomly chosen as "recorded" neurons. Note that the model has access to the behavioral data but not the task variables. Similar to real data, population activity and behavioral variables are normalized.

Benchmark Methods for Functional Connectivity

We compared SYNAPSNET with two benchmark methods for inferring functional connectivity: pair-wise correlation and CURBD (Perich et al., 2020). Pair-wise correlation is a popular statistical method for calculating functional connectivity in neuroscience across various recording modalities. We used variants of this method with delays ($D = 0, 1, 2$) to capture causal interactions and achieve directed FCs. CURBD is an RNN-based model designed to infer inter-region currents by learning functional connectivity in a network of interconnected neurons capable of reproducing real data.

Performance on Recovering Ground-Truth Functional Connectivity

Figure 5b shows the ground-truth FC alongside the inferred FC by each method in a single simulation run, while Figure 5c compares the mean accuracy over 50 runs. SYNAPSNET reconstructed a sparse and asymmetric FC with over 80% accuracy. CURBD, despite being trained to nearly perfectly reproduce the data (explained variance = 0.93), failed to estimate the ground-truth FC. This likely results from CURBD’s RNN overfitting to the data without generalizing the learned FC to a held-out test set. Pair-wise correlation with $D = 1$ partially recovered the true FC, achieving a mean accuracy of 30%.

Notably, SYNAPSNET successfully inferred the ground-truth functional connectivity from synthetic data while its performance in predicting population activity was not perfect, with a correlation score of 36% and a test loss of 0.83, matching its performance on real data. This suggests that SYNAPSNET’s strength in inferring FC is not constrained by the challenges of predicting highly stochastic spiking activity.

4 Limitations

SYNAPSNET is specifically designed to model neuronal populations, which may limit its applicability to other types of neural data. Additional research is necessary to assess its generalizability to modalities where each channel does not correspond to an individual neuron, such as electrocorticography (ECoG). Furthermore, since SYNAPSNET encodes the activity of each neuron separately, architectural modifications are required for tasks other than population activity forecasting, such as neural decoding.

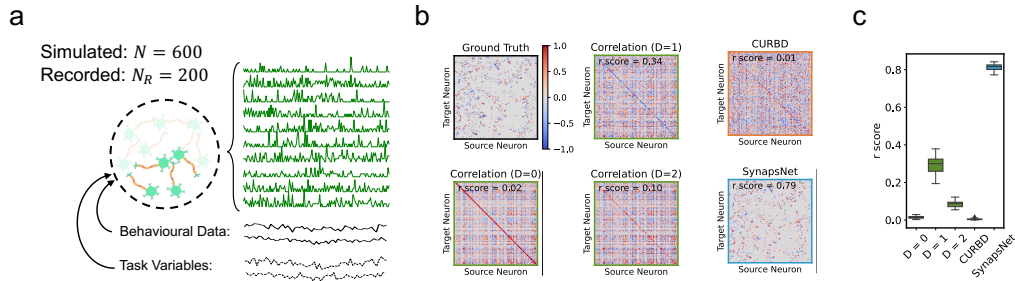


Figure 5: Synthetic data experiment. (a) Simulation process. (b) Functional connectivity matrices inferred using SYNAPSNET and other baselines compared with the ground-truth in a single simulation run. (c) Functional connectivity reconstruction accuracies achieved by each method over 50 runs of simulation with random initializations.

Although our experiments demonstrated promising results in analyzing the functional connectivity and input currents inferred by SYNAPSNET on both real and synthetic data, fully validating the learned connections remains challenging due to the lack of ground-truth anatomical connections in population activity datasets. Therefore, the anatomical translation of SYNAPSNET’s functional connectivity requires future validation.

5 Conclusions

In conclusion, we introduced SYNAPSNET, a biologically inspired deep learning framework that advances neuronal population modeling by combining high predictive performance with interpretability. Our approach addresses the limitations of existing deep learning methods, which often fail to account for the biological mechanisms underlying neuronal activity and offer limited interpretability. Through extensive experiments on publicly available datasets of mouse cortical activity, recorded via calcium imaging and Neuropixels across various tasks, we showed that SYNAPSNET consistently surpassed conventional time-series models in modeling population dynamics. Additionally, our experiments on synthetic data demonstrated SYNAPSNET’s capability in identifying underlying interactions between neurons.

Supplementary Materials

Additional details, the code used to generate the presented results, and the raw data for figures and papers are available at: <https://github.com/SynapsNet/SynapsNet>.

References

- Ali Behrouz, Parsa Delavari, and Farnoosh Hashemi. Unsupervised representation learning of brain activity via bridging voxel activity and functional connectivity. In *Forty-first International Conference on Machine Learning*, 2024.
- Stephane Bugeon, Joshua Duffield, Mario Dipoppa, Anne Ritoux, Isabelle Pranker, Dimitris Nicoloutsopoulos, David Orme, Maxwell Shinn, Han Peng, Hamish Forrest, et al. A transcriptomic axis predicts state modulation of cortical interneurons. *Nature*, 607(7918):330–338, 2022.
- Kyunghyun Cho, Bart Van Merriënboer, Caglar Gulcehre, Dzmitry Bahdanau, Fethi Bougares, Holger Schwenk, and Yoshua Bengio. Learning phrase representations using rnn encoder-decoder for statistical machine translation. *arXiv preprint arXiv:1406.1078*, 2014.
- Parsa Delavari, Gulcenur Ozturan, Lei Yuan, Özgür Yilmaz, and Ipek Oruc. Artificial intelligence, explainability, and the scientific method: A proof-of-concept study on novel retinal biomarker discovery. *PNAS nexus*, 2(9):pgad290, 2023.

- Yuhui Du, Zening Fu, and Vince D Calhoun. Classification and prediction of brain disorders using functional connectivity: promising but challenging. *Frontiers in neuroscience*, 12:373866, 2018.
- Lea Duncker and Maneesh Sahani. Dynamics on the manifold: Identifying computational dynamical activity from neural population recordings. *Current opinion in neurobiology*, 70:163–170, 2021.
- Jeffrey L Elman. Finding structure in time. *Cognitive science*, 14(2):179–211, 1990.
- Karl J Friston. Functional and effective connectivity: a review. *Brain connectivity*, 1(1):13–36, 2011.
- Juan A Gallego, Matthew G Perich, Raeed H Chowdhury, Sara A Solla, and Lee E Miller. Long-term stability of cortical population dynamics underlying consistent behavior. *Nature neuroscience*, 23(2):260–270, 2020.
- Christopher Heelan, Jihun Lee, Ronan O’Shea, Laurie Lynch, David M Brandman, Wilson Truccolo, and Arto V Nurmikko. Decoding speech from spike-based neural population recordings in secondary auditory cortex of non-human primates. *Communications biology*, 2(1):466, 2019.
- Sepp Hochreiter and Jürgen Schmidhuber. Long short-term memory. *Neural computation*, 9(8):1735–1780, 1997.
- Allan L Hodgkin and Andrew F Huxley. Currents carried by sodium and potassium ions through the membrane of the giant axon of loligo. *The Journal of physiology*, 116(4):449, 1952.
- Cole Hurwitz, Nina Kudryashova, Arno Onken, and Matthias H Hennig. Building population models for large-scale neural recordings: Opportunities and pitfalls. *Current opinion in neurobiology*, 70:64–73, 2021.
- James J Jun, Nicholas A Steinmetz, Joshua H Siegle, Daniel J Denman, Marius Bauza, Brian Barbarits, Albert K Lee, Costas A Anastassiou, Alexandru Andrei, Çağatay Aydın, et al. Fully integrated silicon probes for high-density recording of neural activity. *Nature*, 551(7679):232–236, 2017.
- Tim C Kietzmann, Patrick McClure, and Nikolaus Kriegeskorte. Deep neural networks in computational neuroscience. *BioRxiv*, pp. 133504, 2017.
- Pablo Lemos, Niall Jeffrey, Miles Cranmer, Shirley Ho, and Peter Battaglia. Rediscovering orbital mechanics with machine learning. *Machine Learning: Science and Technology*, 4(4):045002, 2023.
- Jingyuan Li, Leo Scholl, Trung Le, Pavithra Rajeswaran, Amy Orsborn, and Eli Shlizerman. Amag: Additive, multiplicative and adaptive graph neural network for forecasting neuron activity. *Advances in Neural Information Processing Systems*, 36, 2024.
- Kaiming Li, Lei Guo, Jingxin Nie, Gang Li, and Tianming Liu. Review of methods for functional brain connectivity detection using fmri. *Computerized medical imaging and graphics*, 33(2):131–139, 2009.
- Laura Marzetti, Alessio Basti, Federico Chella, Antea D’Andrea, Jaakko Syrjälä, and Vittorio Pizzella. Brain functional connectivity through phase coupling of neuronal oscillations: a perspective from magnetoencephalography. *Frontiers in neuroscience*, 13:469179, 2019.
- Lu Mi, Trung Le, Tianxing He, Eli Shlizerman, and Uygur Sümbül. Learning time-invariant representations for individual neurons from population dynamics. *Advances in Neural Information Processing Systems*, 36, 2024.
- Michael Nolan, Bijan Pesaran, Eli Shlizerman, and Amy Orsborn. Multi-block rnn autoencoders enable broadband ecog signal reconstruction. *bioRxiv*, pp. 2022–09, 2022.
- Chethan Pandarinath, Daniel J O’Shea, Jasmine Collins, Rafal Jozefowicz, Sergey D Stavisky, Jonathan C Kao, Eric M Trautmann, Matthew T Kaufman, Stephen I Ryu, Leigh R Hochberg, et al. Inferring single-trial neural population dynamics using sequential auto-encoders. *Nature methods*, 15(10):805–815, 2018.

- Liam Paninski and John P Cunningham. Neural data science: accelerating the experiment-analysis-theory cycle in large-scale neuroscience. *Current opinion in neurobiology*, 50:232–241, 2018.
- Vito Paolo Pastore, Paolo Massobrio, Aleksandar Godjoski, and Sergio Martinoia. Identification of excitatory-inhibitory links and network topology in large-scale neuronal assemblies from multi-electrode recordings. *PLoS computational biology*, 14(8):e1006381, 2018.
- Matthew G Perich, Charlotte Arlt, Sofia Soares, Megan E Young, Clayton P Mosher, Juri Minxha, Eugene Carter, Ueli Rutishauser, Peter H Rudebeck, Christopher D Harvey, et al. Inferring brain-wide interactions using data-constrained recurrent neural network models. *BioRxiv*, pp. 2020–12, 2020.
- Daniele Poli, Vito P Pastore, and Paolo Massobrio. Functional connectivity in in vitro neuronal assemblies. *Frontiers in neural circuits*, 9:57, 2015.
- Christopher J Quinn, Todd P Coleman, Negar Kiyavash, and Nicholas G Hatsopoulos. Estimating the directed information to infer causal relationships in ensemble neural spike train recordings. *Journal of computational neuroscience*, 30:17–44, 2011.
- Atif Riaz, Muhammad Asad, Eduardo Alonso, and Greg Slabaugh. Deepfmri: End-to-end deep learning for functional connectivity and classification of adhd using fmri. *Journal of neuroscience methods*, 335:108506, 2020.
- Blake A Richards, Timothy P Lillicrap, Philippe Beaudoin, Yoshua Bengio, Rafal Bogacz, Amelia Christensen, Claudia Clopath, Rui Ponte Costa, Archy de Berker, Surya Ganguli, et al. A deep learning framework for neuroscience. *Nature neuroscience*, 22(11):1761–1770, 2019.
- Yvette I Sheline and Marcus E Raichle. Resting state functional connectivity in preclinical alzheimer’s disease. *Biological psychiatry*, 74(5):340–347, 2013.
- Joshua H Siegle, Xiaoxuan Jia, Séverine Durand, Sam Gale, Corbett Bennett, Nile Graddis, Gregory Heller, Tamina K Ramirez, Hannah Choi, Jennifer A Luviano, et al. Survey of spiking in the mouse visual system reveals functional hierarchy. *Nature*, 592(7852):86–92, 2021.
- Ian H Stevenson, Brian M London, Emily R Oby, Nicholas A Sachs, Jacob Reimer, Bernhard Englitz, Stephen V David, Shihab A Shamma, Timothy J Blanche, Kenji Mizuseki, et al. Functional connectivity and tuning curves in populations of simultaneously recorded neurons. *PLoS computational biology*, 8(11):e1002775, 2012.
- Carsen Stringer, Marius Pachitariu, Nicholas Steinmetz, Charu Bai Reddy, Matteo Carandini, and Kenneth D Harris. Spontaneous behaviors drive multidimensional, brainwide activity. *Science*, 364(6437):eaav7893, 2019.
- Simona Ullo, Thierry R Nieuw, Diego Sona, Alessandro Maccione, Luca Berdondini, and Vittorio Murino. Functional connectivity estimation over large networks at cellular resolution based on electrophysiological recordings and structural prior. *Frontiers in neuroanatomy*, 8:137, 2014.
- Saurabh Vyas, Matthew D Golub, David Sussillo, and Krishna V Shenoy. Computation through neural population dynamics. *Annual review of neuroscience*, 43:249–275, 2020.
- Francis R Willett, Erin M Kunz, Chaofei Fan, Donald T Avansino, Guy H Wilson, Eun Young Choi, Foram Kamdar, Matthew F Glasser, Leigh R Hochberg, Shaul Druckmann, et al. A high-performance speech neuroprosthesis. *Nature*, 620(7976):1031–1036, 2023.
- Zonghan Wu, Shirui Pan, Guodong Long, Jing Jiang, and Chengqi Zhang. Graph wavenet for deep spatial-temporal graph modeling. *arXiv preprint arXiv:1906.00121*, 2019.
- Meichen Yu. Benchmarking metrics for inferring functional connectivity from multi-channel eeg and meg: A simulation study. *Chaos: An Interdisciplinary Journal of Nonlinear Science*, 30(12), 2020.

A Methods Details

A.1 Training Details and Hyperparameters

For each session of data, we split the population activity into three continuous partitions: approximately 90% for training, 10% for validation, and 10% for testing. The validation set was used to select the epoch with the best performance and to tune hyperparameters, while the test set was reserved for the final evaluation of the models and reporting performance metrics.

For SynapsNet, we used context window size $W = 5$, neuron embedding size of 32, and a single-layer GRU with hidden layer size of 40 as the dynamical model. During training, the training set is divided into identical (but overlapping) partitions of size $W + 1$, where the first W time points are the input and the last time point is the target. For batch sampling, we first select a random session from which all batch samples are chosen. This approach ensures that all samples in a batch have identical dimensionality, simplifying implementation, as different sessions contain different numbers of neurons.

For all datasets, we use a batch size of 32 and an initial learning rate of 10^{-3} . The models are trained for 100 epochs, with the learning rate halved every 10 epochs. Additionally, dropout layers with a rate of 0.1 are employed in all neural networks. SYNAPSNET is implemented using PyTorch in Python, and evaluations are run on a Linux machine with a GPU and 16GB of RAM. Training SYNAPSNET on each session of data (single-session training) takes approximately half an hour, depending on the number of recorded neurons and the session length.

For the sake of fair comparison, we use the same training, validation, and testing data for all benchmark models and ablated versions of SYNAPSNET.

A.2 Models Used for Comparison

The RNN, GRU, and LSTM models each consist of 2 layers with a hidden layer size of 100. The LFADS model we used has the dimensionality of the generator, encoder, and controller all set to 256, and the dimensionality of the factor and inferred inputs to the generator set to 128. The GWNet model is defined with 32 residual channels, 32 dilation channels, 128 skip channels, and 256 end channels, with a single layer, 4 blocks, and a kernel size of 2.

B Additional Results

B.1 Sensitivity Analysis

Effect of Context Window Length on Forecasting Performance. We evaluated the effect of different context window lengths (W) on the forecasting performance of both SYNAPSNET and NeuPRINT (the second-best-performing model). The results for Ca imaging and Neuropixels datasets are presented separately in Figure 6. The context window length determines how far back in the past the model can access neural activity and behavioral data to predict the population’s activity at the next time point. The results indicate that at least two past time steps are required to accurately forecast neural activity, as evidenced by the substantial performance difference between $W = 1$ and $W = 2$. This aligns with the observations made by the authors of NeuPRINT, who identified $W = 2$ as the optimal choice (Mi et al., 2024). Performance plateaus after $W = 5$, with the negligible difference observed among context window sizes of 5, 10, and 20. Therefore, all results reported in the main paper are based on $W = 5$ to maintain model simplicity without significantly sacrificing performance.

Effect of Neuronal Embedding Dimensionality on Forecasting Performance. We investigated the impact of varying neuronal embedding sizes (D) on the forecasting performance of both SYNAPSNET and NeuPRINT. Figure 7 displays the results for the Ca imaging and Neuropixels datasets separately. Our analysis reveals that neuronal embedding dimensionality does not significantly affect neural activity forecasting accuracy. This aligns with the findings from the ablation study (Table 2), which indicated that neuronal embeddings contribute minimally to the performance of SYNAPSNET. Consequently, we opted for $D = 32$ to remain consistent with the choice made by Mi et al. (2024).

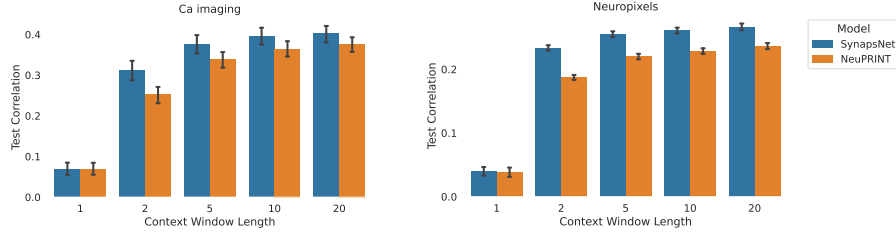


Figure 6: Sensitivity Analysis of Context Window Length (W). Test correlation scores for different context window lengths are plotted separately for the Ca imaging dataset (a) and the Neuropixels dataset (b).

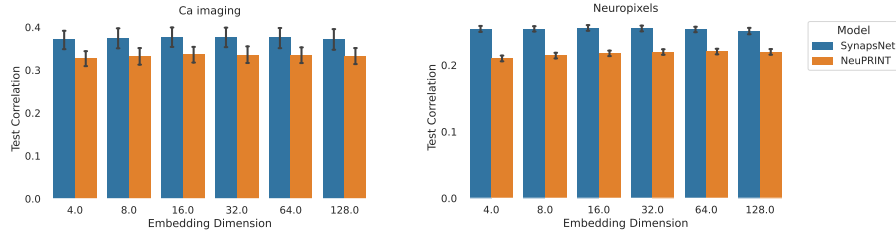


Figure 7: Sensitivity Analysis of Neuronal Embedding Dimensionality (D). Test correlation scores for different neuronal embedding sizes are plotted separately for the Ca imaging dataset (a) and the Neuropixels dataset (b).

Effect of Using Different Sequential Models on Forecasting Performance.

We explored four different architectures for the SYNAPSNET’s dynamical model—RNN, GRU, LSTM, and Transformer—to assess their impact on the model’s performance. The results for each architecture are detailed in Table 3 (we only used natural scenes task for simplicity). Among these, the GRU architecture achieved the highest correlation score across both data modalities, leading us to base all the results presented in this paper on the GRU dynamical model.

Table 3: Sensitivity Analysis of the dynamical model’s architecture. Test correlation scores for different neuronal embedding sizes are reported separately for the Ca imaging dataset and the Neuropixels dataset.

Data Modality	Dynamical Model	Natural Scenes	
		<i>Corr</i> (%) \uparrow	<i>Loss</i> \downarrow
Ca Imaging	RNN	36.99 \pm 1.05	0.787 \pm 0.033
	GRU	37.43 \pm 1.05	0.846 \pm 0.037
	LSTM	37.23 \pm 1.09	0.786 \pm 0.033
	Transformer (one-layer)	29.83 \pm 1.86	0.802 \pm 0.036
	Transformer (two-layer)	27.35 \pm 2.48	0.826 \pm 0.039
Neuropixels	RNN	24.04 \pm 0.26	0.927 \pm 0.012
	GRU	24.38 \pm 0.28	0.926 \pm 0.011
	LSTM	23.91 \pm 0.29	0.927 \pm 0.012
	Transformer (one-layer)	20.67 \pm 1.32	0.917 \pm 0.023
	Transformer (two-layer)	22.00 \pm 1.18	0.876 \pm 0.012

\dagger The bold values correspond to the largest drop in the performance metric separately for multi-/single-session training and each data modality.